JACS
JOURNAL OF THE AMERICAN CHEMICAL SOCIETY

Communication

pubs.acs.org/JACS

Contraction and Expansion of Stimuli-Responsive DNA Bonds in Flexible Colloidal Crystals

Jarad A. Mason,[†,‡] Christine R. Laramy,[‡,§] Cheng-Tsung Lai,[†,‡] Matthew N. O'Brien,[†,‡] Qing-Yuan Lin,[‡,∥] Vinayak P. Dravid,[‡,∥] George C. Schatz,[†,‡] and Chad A. Mirkin*[,†,‡,§,∥]

[†]Department of Chemistry, [‡]International Institute for Nanotechnology, [§]Department of Chemical and Biological Engineering, and [∥]Department of Materials Science and Engineering, Northwestern University, Evanston, Illinois 60208, United States

Supporting Information

ABSTRACT: DNA surface ligands can be used as programmable "bonds" to control the arrangement of nanoparticles into crystalline superlattices. Here, we study the intrinsic responsiveness of these DNA bonds to changes in local dielectric constant (ε_r) as a new approach to dynamically modulate superlattice structure. Remarkably, ethanol (EtOH) addition can be used to controllably tune DNA bond length from 16 to 3 nm and to increase bond stability by >40 °C, while retaining long-range order and crystal habit. Interestingly, we find that these structural changes, which involve the expansion and contraction of crystals by up to 75% in volume, occur in a cooperative fashion once a critical percentage of EtOH is reached. These results provide a facile and robust approach to create stimuli-responsive lattices, to access high volume fractions, and to improve thermal stability.

Due to their highly tunable structure and sequence-specific interactions, nucleic acids have emerged as powerful surface ligands to direct the assembly of nanoparticles into one-, two-, and three-dimensional colloidal crystals.[1] In this context, nanoparticles coated with a dense shell of nucleic acids function as programmable atom equivalents (PAEs), where nucleic acid "bonds" arrange nanoparticle "atoms" into superlattices with precisely defined spacing, symmetry, and, in some cases, crystal habit.[2] Because many physical properties of nanoparticles are dramatically affected by the location and arrangement of neighboring nanoparticles, the high level of structural control afforded by this approach is extremely useful for the synthesis of both fundamentally interesting and functional materials.[1f]

While significant advances have been made in the structural control of DNA-assembled colloidal crystals,[3] less is known about the physical and chemical properties of the DNA bonds within these crystals and of their intrinsic ability to change in response to external stimuli. The use of external stimuli to postsynthetically tune DNA bond length and strength is particularly intriguing for the development of responsive colloidal crystals, where material properties can be changed on-demand.[4] Several strategies have been developed to introduce such dynamic control, including the use of DNA hairpins, molecular intercalators, osmotic pressure, and solvent evaporation techniques.[5] While each approach possesses certain advantages, there are still no general methods that allow DNA bonds to be rapidly, precisely, and reversibly tuned over a wide range of lengths and strengths.

Although many techniques have been developed to manipulate the structure of free DNA,[6] few of these have been adapted to postsynthetically modify DNA bonds in nanoparticle superlattices. For instance, the effect of alcohols on the structure and hybridization interactions of double-stranded DNA has been the subject of many detailed experimental and theoretical studies,[7] and ethanol (EtOH) precipitation reactions are routinely used in molecular biology laboratories to purify and concentrate DNA extracted from cells.[8] Inspired by the ability of EtOH to modulate the intra- and interhelical structure of free DNA, we hypothesized that EtOH could be similarly used to provide a convenient and controllable external stimulus to induce structural changes in DNA-assembled colloidal crystals (Figure 1). In particular, one would expect that DNA bonds in high salt concentration solutions should be sensitive to changes in solvent ε_r and, perhaps, be able to undergo an EtOH-induced precipitation reaction, even when confined inside a superlattice.

In a conventional EtOH precipitation, DNA is dissolved in an aqueous salt solution (~0.3 M NaOAc or NaCl), and the solution is brought to 65−75% EtOH. As a less polar molecule, EtOH cannot solvate charged species as effectively as H_2O, and the solvent ε_r decreases as EtOH is added (Figure 1B).[9] As a result, the Coulombic attraction between the positively charged Na^+ ions in solution and the negatively charged PO_4^- groups of the DNA backbone increases to such an extent that ionic bonds form, neutralizing the charge on the DNA backbone and inducing precipitation.[10] Depending on the salt concentration, addition of EtOH can also cause double-stranded DNA to transition from the B-form to A-form, with a concurrent ~25% decrease in DNA length, prior to precipitation.[7b,c]

To investigate the ability of EtOH to postsynthetically modulate DNA bonds, two populations of 30 nm diameter spherical PAEs were prepared, designed to specifically interact with each other via complementary DNA sequences (Figure S1). Slow cooling of these samples through their melting temperature resulted in single crystalline body-centered cubic (bcc) superlattices with well-defined rhombic dodecahedron habits.[1e,11] Prior to EtOH addition, crystals were washed repeatedly with 0.3 M NaCl (aq) to remove any excess DNA, nanoparticles, buffers, and surfactants from solution. Crystals

Received: May 26, 2016
Published: July 12, 2016

DOI: 10.1021/jacs.6b05430
J. Am. Chem. Soc. 2016, 138, 8722−8725

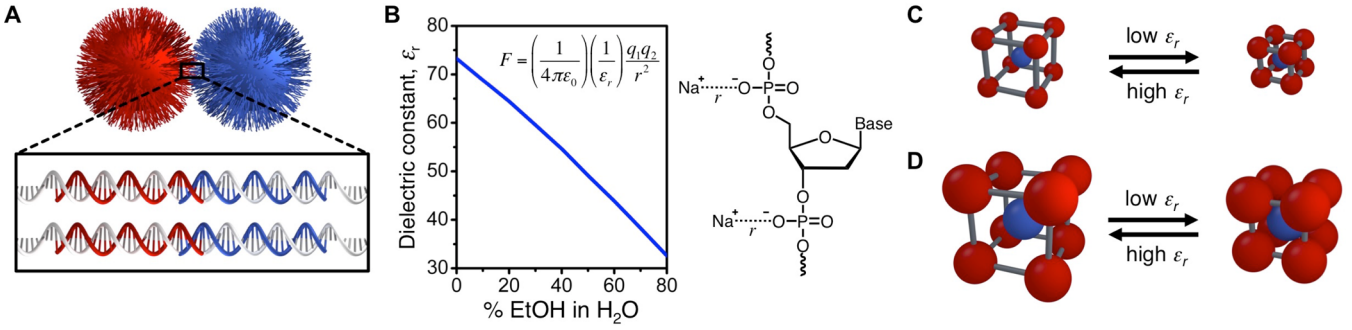

Figure 1. (A) DNA-functionalized nanoparticles can be assembled through complementary hybridization interactions that collectively form DNA "bonds". (B) The dielectric constant, ε_r, of H_2O decreases as EtOH is added,[9] leading to a greater Coulombic force, F, between the negatively charged PO_4^- backbone of DNA and positively charged Na^+ ions in solution. (C, D) Scheme illustrating the EtOH-induced contraction and expansion of bcc superlattices composed of 15 nm (C) or 30 nm (D) spherical nanoparticles.

were then partitioned and brought to different volume percentages of EtOH in H_2O, ranging from ε_r = 73.3 at 0% EtOH to ε_r = 32.6 at 80% EtOH, at a constant 0.3 M NaCl. Superlattices were then characterized by *in situ* small-angle X-ray scattering (SAXS), electron microscopy (EM), and variable-temperature UV−vis spectroscopy.

To examine the effect of EtOH on DNA bond length, unit cell parameters were determined from the comparison of experimental and modeled SAXS patterns, and these values were used to calculate the minimum distance between nanoparticle surfaces.[12] Initially, SAXS data show a small, continuous contraction of the bcc unit cell of 13% by volume as the amount of EtOH is increased from 0 to 30% (Figure 2).

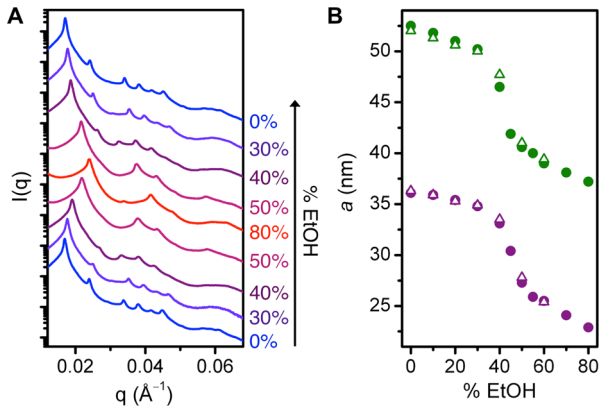

Figure 2. (A) SAXS data for bcc superlattices of 30 nm PAEs at different volume percentages of EtOH in H_2O. (B) The bcc unit cell length, a, for superlattices of 30 nm PAEs (green) and 15 nm PAEs (purple) at different volume percentages of EtOH in H_2O. Solid and empty symbols correspond to values during contraction and re-expansion, respectively.

Once the percentage of EtOH rises above 30%, however, there is a dramatic contraction of the unit cell that is suggestive of a cooperative phase transition. Specifically, the unit cell volume decreases by 42% when increasing from 30% to 45% EtOH, and the average gap between nanoparticles, or effective "DNA bond length", decreases from 14 to 7 nm. After the sharp transition, the superlattice continues to moderately contract as more EtOH is added, reaching a gap distance of only 3 nm—an 80% decrease from the original DNA bond length—at 80% EtOH. Note that this is much greater than the ∼25% contraction expected for a classical transition from B-DNA to A-DNA.[7c] Moreover, access to this distance regime is particularly important to realize materials with strong magnetic and optical coupling and has been challenging with existing DNA-mediated assembly techniques.[13]

Despite the large contraction, SAXS data show that, regardless of the amount of EtOH added, PAEs are still arranged in a well-ordered bcc lattice. This ordering was further confirmed by directly imaging superlattices at 0%, 41%, and 80% EtOH using EM, with crystals embedded in silica to preserve the solution-phase DNA bonds in the solid state (Figure 3).[14] Significantly, EM images also demonstrate that the well-defined rhombic dodecahedron habit is preserved after EtOH addition.

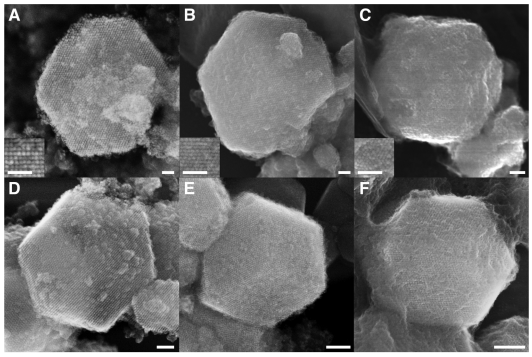

Figure 3. Top: Scanning electron microscopy (SEM) images of silica-encapsulated superlattices of 30 nm PAEs at (A) 0%, (B) 41%, and (C) 80% EtOH confirm rhombic dodecahedron crystal habits. Insets: High-magnification SEM images. Bottom: SEM images of silica-encapsulated superlattices of 15 nm PAEs at (D) 0%, (E) 45%, and (F) 80% EtOH. Scale bars, 200 nm.

Remarkably, the EtOH-induced transition is fully reversible, and SAXS patterns collected before and after exposure to 80% EtOH possess no noticeable changes (Figure 2A). To investigate how this reversibility holds up to many cycles of expansion and contraction, a single sample was transitioned repeatedly between 0% and 80% EtOH. Significantly, SAXS data did not indicate any changes in crystallinity after five complete cycles (Figure S24). In all contracted phases, there is, however, a noticeable increase in SAXS peaks widths, which is typically indicative of an increase in lattice strain or decrease in effective crystallite size.[12] Since the SAXS peak widths return to their original values upon re-expansion, this effect can be

DOI: 10.1021/jacs.6b05430
J. Am. Chem. Soc. 2016, 138, 8722−8725

predominantly attributed to increased lattice strain in the contracted phases.

To characterize the effects of EtOH on DNA "bond strength", we used UV−vis spectroscopy measurements of extinction to determine the temperature at which superlattice crystals dissociate, or melt, into discrete nanoparticles (Figures S45, S46).[15] As the percentage of EtOH is increased, the melting temperature of the superlattice slowly decreases from 41.1 °C at 0% EtOH to 33.1 °C at 30% EtOH (Figure 4A).

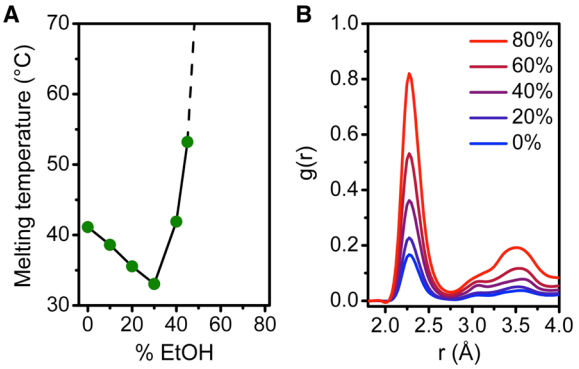

Figure 4. (A) Melting temperatures for bcc superlattices of 30 nm PAEs at different volume percentages of EtOH in H_2O. (B) Simulated radial distribution function, g(r), of the distance, r, between Na^+ and PO_4^- groups at different EtOH percentages.

This can be attributed to weaker DNA hybridization interactions as ε_r and the bulk solvent polarity decrease.[7b] At 40−45% EtOH the melting transition begins to broaden, and the melting temperature rapidly increases. After the solution reaches 50% EtOH, we no longer observe evidence of melting by UV−vis analysis over the 20 to 70 °C temperature range. *In situ* SAXS experiments further reveal that the bcc crystal structure is intact to at least 80 °C in 80% EtOH (Figure S44). This dramatically increased thermal stability after the phase transition is consistent with an EtOH-induced DNA precipitation reaction occurring inside the superlattice to increase the collective stability of DNA bonds.

To evaluate the effect of nanoparticle size on the ability of EtOH to modulate DNA bonds, crystals were similarly prepared using 15 nm diameter spherical PAEs. While *in situ* SAXS experiments indicate that the superlattice undergoes a similar phase transition in response to EtOH (Figure 2B), the crystallinities of the contracted phases are reduced compared to those of the 30 nm PAEs (Figures S25−S42). Still, SAXS simulations and EM images confirm that the 15 nm PAEs contract by 75% in volume to a strained bcc lattice, with a decrease in DNA bond length from 17 to 6 nm, as the EtOH percentage is increased from 0% to 80%. Interestingly, the midpoint of the phase transition for 15 nm PAEs occurs at 45% EtOH compared to 41% EtOH for 30 nm PAEs. Since 15 and 30 nm PAEs are expected to have a similar DNA surface coverage,[16] the increased amount of EtOH required to induce the transition in 15 nm PAEs can likely be attributed to a radius of curvature effect.[17] Specifically, the lower radius of curvature of the 30 nm PAEs leads to a smaller average distance between duplexed DNA strands above the surface. This should lead to a higher local salt concentration around the PO_4^- backbones and, consequently, less EtOH required for Na^+ cations to fully neutralize the DNA backbones and induce a precipitation transition.

All-atom molecular dynamics (MD) simulations were performed to gain additional insight into the mechanism of the EtOH-induced superlattice contraction. Below 80% EtOH, simulations show that the DNA conformation remains exclusively in the B-form, and the sharp contraction at 40−45% EtOH cannot, therefore, be attributed to a transition from B-DNA to A-DNA. Instead, the contraction likely results from changes in the spacing and arrangement of DNA strands relative to each other. It is important to consider that the DNA bonds between nanoparticles have single-stranded regions of DNA that impart substantial conformational flexibility, and the MD simulations show a significant bending angle of 70° at the center of the DNA bond at 40% EtOH (Figure S2). This bending should allow neighboring DNA strands to pack more tightly between nanoparticle surfaces and, in so doing, draw the nanoparticles closer together.

Current computational methods, including both MD and coarse-grained simulations, are not capable of capturing the large contraction that occurs above 40% EtOH. Based on studies of free DNA in solution, however, it is reasonable to assume that after ε_r decreases below a critical value, Na^+ cations in solution effectively form ionic bonds with the PO_4^- groups of the DNA backbone,[18] leading to counterion correlations between neighboring DNA strands that trigger DNA−DNA attractions and cause DNA strands to rearrange into a more condensed phase.[7f] Indeed, MD simulations confirm an increased local concentration of Na^+ ions around PO_4^- groups with increasing EtOH (Figure 4B). While it is exceedingly difficult to determine the exact structure and chemical nature of DNA bonds in the contracted superlattice phases with existing experimental techniques, condensed DNA is known to adopt a range of liquid crystalline and crystalline phases.[19]

Taken together, these results demonstrate the intrinsic responsiveness of nanoparticle-based DNA bonds and provide a powerful general approach to the synthesis of responsive colloidal crystals with precisely controlled interparticle distances and increased thermal stability. The extension of this work to different alcohols, multivalent cations, DNA sequences, and nonspherical nanoparticle shapes should enhance our fundamental understanding of condensed DNA bonds and lead to new possibilities for the postsynthetic manipulation of superlattice structures. This ability to rapidly, predictably, and reversibly modulate DNA bonds has great potential for the development of dynamic materials with optical,[20] magnetic, and mechanical properties that can be tuned on-demand.

■ ASSOCIATED CONTENT

Supporting Information

The Supporting Information is available free of charge on the ACS Publications website at DOI: 10.1021/jacs.6b05430.

Complete experimental details, MD simulations, SAXS data and simulations, UV−vis spectra, additional EM images (PDF)

■ AUTHOR INFORMATION

Corresponding Author

*chadnano@northwestern.edu

Notes

The authors declare no competing financial interest.

DOI: 10.1021/jacs.6b05430
J. Am. Chem. Soc. 2016, 138, 8722−8725

■ ACKNOWLEDGMENTS

This material is based upon work supported by the Air Force Office of Scientific Research under awards: FA9550-11-1-0275, FA9550-12-1-0280, FA9550-14-1-0274; and the National Science Foundation award CHE-1465045. SAXS experiments were carried out at the Dupont−Northwestern−Dow Collaborative Access Team beamline at the Advanced Photon Source (APS) at Argonne National Laboratory, and use of the APS was supported by the DoE (DE-AC02-06CH11357). This work made use of the EPIC facility of the NUANCE Center at Northwestern University, which has received support from the Soft and Hybrid Nanotechnology Experimental (SHyNE) Resource (NSF NNCI-1542205); the MRSEC program (NSF DMR-1121262) at the Materials Research Center; the International Institute for Nanotechnology (IIN); the Keck Foundation; and the State of Illinois, through the IIN. C.R.L. and M.N.O. gratefully acknowledge the National Science Foundation for a Graduate Research Fellowship, and J.A.M. gratefully acknowledges support from Northwestern University's International Institute for Nanotechnology. We thank Prof. Monica Olvera de la Cruz and Dr. Mike Ross for helpful discussions.

■ REFERENCES

(1) (a) Mirkin, C. A.; Letsinger, R. L.; Mucic, R. C.; Storhoff, J. J. *Nature* **1996**, *382*, 607. (b) Alivisatos, A. P.; Johnsson, K. P.; Peng, X.; Wilson, T. E.; Loweth, C. J.; Bruchez, M. P.; Schultz, P. G. *Nature* **1996**, *382*, 609. (c) Park, S. Y.; Lytton-Jean, A. K. R.; Lee, B.; Weigand, S.; Schatz, G. C.; Mirkin, C. A. *Nature* **2008**, *451*, 553. (d) Nykypanchuk, D.; Maye, M. M.; van der Lelie, D.; Gang, O. *Nature* **2008**, *451*, 549. (e) Macfarlane, R. J.; Lee, B.; Jones, M. R.; Harris, N.; Schatz, G. C.; Mirkin, C. A. *Science* **2011**, *334*, 204. (f) Jones, M. R.; Seeman, N. C.; Mirkin, C. A. *Science* **2015**, *347*, 1260901.

(2) Macfarlane, R. J.; O'Brien, M. N.; Petrosko, S. H.; Mirkin, C. A. *Angew. Chem., Int. Ed.* **2013**, *52*, 5688.

(3) (a) O'Brien, M. N.; Jones, M. R.; Lee, B.; Mirkin, C. A. *Nat. Mater.* **2015**, *14*, 833. (b) Liu, W.; Tagawa, M.; Xin, H. L.; Wang, T.; Emamy, H.; Li, H.; Yager, K. G.; Starr, F. W.; Tkachenko, A. V.; Gang, O. *Science* **2016**, *351*, 582.

(4) (a) Sebba, D. S.; Mock, J. J.; Smith, D. R.; LaBean, T. H.; Lazarides, A. A. *Nano Lett.* **2008**, *8*, 1803. (b) Xiong, H.; Sfeir, M. Y.; Gang, O. *Nano Lett.* **2010**, *10*, 4456.

(5) (a) Leunissen, M. E.; Dreyfus, R.; Cheong, F. C.; Grier, D. G.; Sha, R.; Seeman, N. C.; Chaikin, P. M. *Nat. Mater.* **2009**, *8*, 590. (b) Maye, M. M.; Kumara, M. T.; Nykypanchuk, D.; Sherman, W. B.; Gang, O. *Nat. Nanotechnol.* **2010**, *5*, 116. (c) Kim, Y.; Macfarlane, R. J.; Mirkin, C. A. *J. Am. Chem. Soc.* **2013**, *135*, 10342. (d) Macfarlane, R. J.; Jones, M. R.; Lee, B.; Auyeung, E.; Mirkin, C. A. *Science* **2013**, *341*, 1222. (e) Srivastava, S.; Nykypanchuk, D.; Maye, M. M.; Tkachenko, A. V.; Gang, O. *Soft Matter* **2013**, *9*, 10452. (f) Radha, B.; Senesi, A. J.; O'Brien, M. N.; Wang, M. X.; Auyeung, E.; Lee, B.; Mirkin, C. A. *Nano Lett.* **2014**, *14*, 2162. (g) Srivastava, S.; Nykypanchuk, D.; Fukuto, M.; Gang, O. *ACS Nano* **2014**, *8*, 9857. (h) Pal, S.; Zhang, Y.; Kumar, S. K.; Gang, O. *J. Am. Chem. Soc.* **2015**, *137*, 4030. (i) Rogers, W. B.; Manoharan, V. N. *Science* **2015**, *347*, 639. (j) Seo, S. E.; Wang, M. X.; Shade, C. M.; Rouge, J. L.; Brown, K. A.; Mirkin, C. A. *ACS Nano* **2016**, *10*, 1771. (k) Kim, Y.; Macfarlane, R. J.; Jones, M. R.; Mirkin, C. A. *Science* **2016**, *351*, 579.

(6) Dickerson, R. E. *Methods Enzymol.* **1992**, *211*, 67.

(7) (a) Potaman, V. N.; Bannikov, Y. A.; Shlyachtenko, L. S. *Nucleic Acids Res.* **1980**, *8*, 635. (b) Piškur, J.; Rupprecht, A. *FEBS Lett.* **1995**, *375*, 174. (c) Vargason, J. M.; Henderson, K.; Ho, P. S. *Proc. Natl. Acad. Sci. U. S. A.* **2001**, *98*, 7265. (d) Jose, D.; Porschke, D. *Nucleic Acids Res.* **2004**, *32*, 2251. (e) Smith, B. D.; Liu, J. *J. Am. Chem. Soc.* **2010**, *132*, 6300. (f) Teif, V. B.; Bohinc, K. *Prog. Biophys. Mol. Biol.* **2011**, *105*, 208. (g) Lee, O.-S.; Cho, V. Y.; Schatz, G. C. *J. Phys. Chem. B* **2012**, *116*, 7000.

(8) Bowtell, D. D. L. *Anal. Biochem.* **1987**, *162*, 463.

(9) Wyman, J. *J. Am. Chem. Soc.* **1931**, *53*, 3292.

(10) Eickbush, T. H.; Moudrianakis, E. N. *Cell* **1978**, *13*, 295.

(11) Auyeung, E.; Li, T. I. N. G.; Senesi, A. J.; Schmucker, A. L.; Pals, B. C.; de la Cruz, M. O.; Mirkin, C. A. *Nature* **2014**, *505*, 73.

(12) Senesi, A. J.; Lee, B. *J. Appl. Crystallogr.* **2015**, *48*, 1172.

(13) Senesi, A. J.; Eichelsdoerfer, D. J.; Brown, K. A.; Lee, B.; Quyeung, E.; Choi, C. H. J.; Macfarlane, R. J.; Young, K. L.; Mirkin, C. A. *Adv. Mater.* **2014**, *26*, 7235.

(14) Auyeung, E.; Macfarlane, R. J.; Choi, C. H. J.; Cutler, J. L.; Mirkin, C. A. *Adv. Mater.* **2012**, *24*, 5181.

(15) (a) Jin, R. C.; Wu, G. S.; Li, Z.; Mirkin, C. A.; Schatz, G. C. *J. Am. Chem. Soc.* **2003**, *125*, 1643. (b) O'Brien, M. N.; Brown, K. A.; Mirkin, C. A. *ACS Nano* **2016**, *10*, 1363.

(16) Hurst, S. J.; Lytton-Jean, A. K. R.; Mirkin, C. A. *Anal. Chem.* **2006**, *78*, 8313.

(17) Zwanikken, J. W.; Guo, P.; Mirkin, C. A.; de la Cruz, M. O. *J. Phys. Chem. C* **2011**, *115*, 16368.

(18) (a) Manning, G. S. *Q. Rev. Biophys.* **1978**, *11*, 179. (b) Rudd, L.; Lee, D. J.; Kornyshev, A. A. *J. Phys.: Condens. Matter* **2007**, *19*, 416103.

(19) Livolant, F.; Leforestier, A. *Prog. Polym. Sci.* **1996**, *21*, 1115.

(20) Ross, M. B.; Ku, J. C.; Vaccarezza, V. M.; Schatz, G. C.; Mirkin, C. A. *Nat. Nanotechnol.* **2015**, *10*, 453.

DOI: 10.1021/jacs.6b05430
J. Am. Chem. Soc. 2016, 138, 8722−8725